AFDEX
Adviser for metal Forming process Design EXpert

NEWSLETTER

MFRC
Metal Forming Research Corporation

2025
Vol. 1

www.afdex.com mfrc@afdex.com T. +82-55-755-7529 F. +82-55-761-7529

CONTENTS

Feature topic

1. Friction and lubrication regime changes

In the field of metal forming, it is important to pay attention to the views of Professor Wilson, who has conducted extensive practical research on lubrication. In his paper on friction and lubrication in bulk metal forming, with a focus on lubrication regime change, he argues the following facts. The lubrication state at the contact surface in metal forming is classified into four regimes: thick-film lubrication, thin-film lubrication, mixed lubrication, and boundary lubrication. During metal forming processes where severe deformation occurs, the lubrication regime at the material-die contact surface undergoes changes. Specifically, thick-film lubrication transitions to thin-film lubrication, thin-film lubrication transitions to mixed lubrication, and mixed lubrication further develops into boundary lubrication.

Wilson also harshly criticizes the traditional Coulomb friction law and the constant shear friction law, which are commonly used in process analysis for metal forming. He argues that such friction states do not exist in bulk metal forming, such as in forging. He refrains from going into detail, considering those who rely on methods like the upper-bound method and other analytical methods for applying the constant shear friction law to be scholars who are not thoroughly grounded in practical understanding. The constant shear friction law is interpreted as no longer worth considering in these contexts.

Moreover, Wilson sharply criticizes the widespread, uncritical use of the Coulomb friction law, which is defined by a constant friction coefficient, by many researchers in metal forming. He traces this tendency back to the education received by many in their youth, likely reflecting the early experiences with static mechanics or practical friction laws in screw fastening problems. According to Wilson, the traditional Coulomb friction law is appropriate only for boundary friction (no lubrication) when the pressure is low. He suggests that screw fastening problems are an example where the traditional Coulomb friction law might be considered appropriate, but finding such conditions in metal forming is difficult.

Recent studies have shown that during forging, the lubrication state can change rapidly. On well-lubricated surfaces where the lubrication film is intact, friction is negligible, but on surfaces where the lubrication film is severely damaged, friction becomes extreme and may only be explainable through boundary lubrication. In particular, during forging, which depends on compressive loads, the material-die contact surface undergoes dramatic lubrication regime changes. In these cases, the friction coefficient must

change according to the lubrication state at the contact surface in order for the Coulomb friction law to adequately reflect the situation. The constant shear friction law is inadequate for expressing this friction state. As Wilson argues, the constant shear friction law is intended more for theorists using methods like the upper-bound method, and its use is not recommended.

Let's further explore the problem of traditional Coulomb friction law in forward extrusion, a common process in forging. As shown in Figure 1.1, the multi-step cold forward extrusion process should account for lubrication regime changes, which influence the friction coefficient at the material-die contact. When a constant friction coefficient is used above a certain threshold in this type of multi-step extrusion process, plastic deformation of the material can occur near the inlet. However, this is not the case if the lubrication is sufficiently good. Joun et al. [5] solved this problem by using different friction coefficients for different locations, considering lubrication regime changes. However, the unrealistic approach of applying specific friction coefficients to specific regions should be avoided.

Using the traditional Coulomb friction law in this case inevitably leads to high friction near the exit, increasing pressure sequentially from the exit to the inlet, which creates a vicious cycle. Specifically, pressure near the inlet increases as friction increases, ultimately causing plastic deformation of the material near the inlet. This phenomenon, however, does not match real-world situations unless the friction is excessively high. While high friction at the exit may lead to burnished surfaces at the extrudate's tip, significant plastic deformation near the inlet is rarely observed when lubrication is adequate.

This phenomenon is unrelated to the fundamental issues with the Coulomb friction law. To visualize this, simulations of a multi-step cold forward extrusion process were performed using finite element analysis.

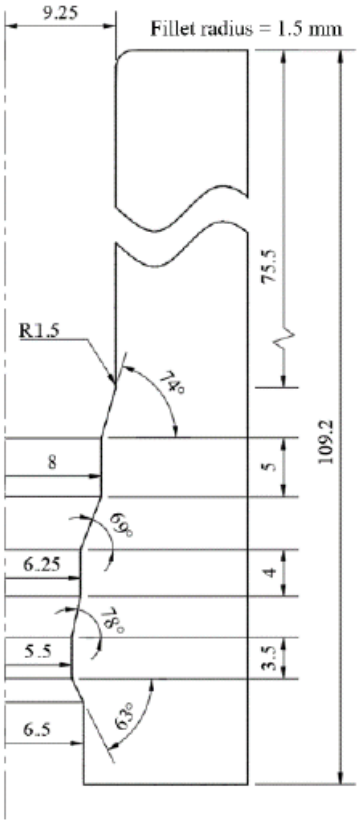

Fig. 1.1 Three-step forward extrusion process

The following material properties were used:

- Material flow stress: $\sigma = 50.3(1 + 20\varepsilon)^{0.26}$ Mpa — Rigid die
- Young's modulus: 90,000 MPa; Poisson's ratio: 0.3 — Ram speed: 1 mm/s
- Friction: Case (1): constant friction coefficient $\mu = 0.1$
  Case (2): friction coefficient defined as a piecewise linear function dependent on strain (ε, μ): (0, 0.01); (0.3, 0.03); (0.5, 0.05); (1.0, 0.1); (2.0, 0.2)

A finite element mesh consisting of 5,500 uniform square elements (with each element having dimensions of 0.24 mm in the radial direction and 0.43 mm in the axial direction) was used. To directly observe any potential surface shearing that might occur at the material's upper surface, the mesh reconstruction feature was turned off. The effective strain and grid distortion at the upper surface of the material at the final stroke are shown in Figure 1.2. In Case (1), surface shearing of the material's upper layer occurred due to the increased pressure at the entrance as the material's leading edge touched the third step, along with the high friction coefficient that was input. On the other hand, in Case (2), despite the maximum friction coefficient exceeding 0.18 at the third step, no plastic deformation occurred at the material surface inside the container, and the friction coefficient at the contact surface inside the container remained low. As a result, the rigid translational motion of the material inside the container remained consistent throughout the process.

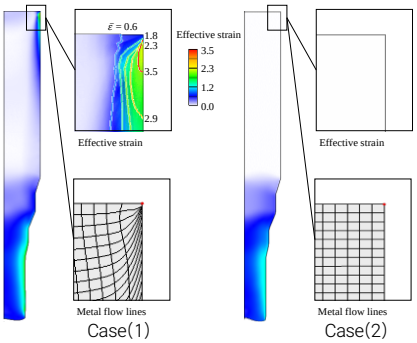

Fig. 1.2 Effective strain rate

In reality, the lubricating film coated on the material is known not to cause significant damage inside the container during the cold forward extrusion process. Based on experience, even if no distinct plastic deformation occurs inside the container and at the first extrusion step, the material's surface typically undergoes severe damage and scratching by the third extrusion step. Since the undamaged lubricating film at the contact surface between the material and the die maintains low friction, the frictional stress does not generate enough pressure at the container's entrance to cause plastic deformation. However, lubricating film damage at the exit can be critical due to significant frictional stress and excessive heat. This frictional phenomenon indicates that significant changes in lubrication regimes occur when the cross-sectional reduction rate is high throughout the cold forward extrusion process. In such cases, the friction coefficient should be high at the exit and low at the entrance, making it inevitable for the friction coefficient to change depending on the state of the contact surface.

The method used in Case (2) easily solved the excessive friction problem of the traditional Coulomb friction law by simply expressing the extent of lubricant degradation as a function of surface strain. This case emphasizes the need for the friction coefficient to change in accordance with changes in the state of the contact surface to reflect the changes in the lubrication regime. Therefore, Case (2) effectively illustrates the changes in lubrication regimes step by step, emphasizing the importance of friction models and friction coefficients to account for these changes.

Since the effective strain at all contact surfaces in Case (2) is directly related to the degradation of the lubricant, it is highly useful in explaining lubrication regime changes. In actual forging, substantial deformation can occur on the surface without direct contact with the die. In this case, since the deformation does not accelerate the degradation of the lubricant, it might not be realistic to treat the friction coefficient as a function of surface strain. Therefore, quantifying the extent of lubricant degradation on the contact surface is essential.

On the other hand, when using a constant shear friction law, the predicted results of this process may appear favorable compared to the traditional Coulomb friction law. This is because, due to the characteristics of the constant shear friction law, shear stress is determined regardless of pressure, preventing the material inside the container from reaching a yielding state. However, generally, the results pose problems from three perspectives. First, there is a fundamental issue where the relatively high frictional stress at the exit cannot be accurately expressed. Based on such results, it would not be possible to discuss die wear. Second, despite this, there is a high likelihood of the forming load being overestimated. This is due to the overestimation of the friction state inside the container. Third, when friction is excessive, plastic deformation may occur at the entrance, making extrusion impossible, but this cannot be predicted using the constant shear friction law.

In conclusion, analyzing the cold forward extrusion process with a relatively large cross-sectional reduction rate may seem geometrically simple, but it is a complex problem when considered from the lubrication and friction perspectives. This complexity arises from changes in lubrication regimes. To easily reflect these changes in lubrication regimes, AFDEX introduced variable Coulomb friction coefficients and variable friction constants. Currently, these are considered as functions of strain, temperature, strain rate, etc., but further research on methods for directly expressing lubricant degradation may be necessary.

Generally, both friction coefficients and friction constants are treated as constants. However, since the lubricating film on the lubricated material deteriorates during plastic deformation, these values change. They are also affected by temperature and pressure. To account for this phenomenon, the friction coefficient is considered a function of temperature, pressure, and material strain, as shown below:

$$\mu = \mu_0 \, W\_T(T) \, W\_P(P) \, W\_E(\bar{\varepsilon}) \quad (1)$$

Here, the functions W_T (T), W_P (P), and W_E ($\bar{\varepsilon}$) can be expressed by various functions, including piecewise linear functions. The use of this friction coefficient is called the variable Coulomb friction law. In other words, the variable Coulomb friction law refers to the use of equation (1), which expresses the friction coefficient as a function of state variables. Determining the dependence of the friction coefficient on state variables is not straightforward. However, when the damage to the lubricating film or lubricant during metal forming processing is significant and cannot be ignored, the relationship between the friction coefficient and the state variables in equation (1) must be applied. The same method can also be applied to the constant shear friction law [6].

For example, the deformation shape of the aluminum hot forging product shown in Figure 1.3(a) cannot be predicted using the traditional Coulomb friction law. Even when using the constant shear friction law, the results are similar. Figure 1.3(b) shows the results obtained by applying the traditional friction law with hot spot plastic finite element analysis, where the lateral shape of the observed target clearly differs from the experimental results.

To form this product, a lubricating film is applied to the material. This lubricating film performs its lubricating function faithfully until a certain condition is met. Once for his limit is reached, the lubricating performance is lost or significantly reduced. The factor determining the performance of this lubricating film is assumed to be the strain on the material at the contact surface.

When the critical surface strain is reached, the friction coefficient is assumed to increase significantly. The results of this process simulation, as shown in Figure 1.3(c), closely resemble the experimental outcomes. It was visually confirmed that in the contact area where the actual strain exceeded the critical surface strain, the lubricating film was severely damaged, and boundary lubrication occurred, where the material and die directly contacted. On the other hand, as seen in Figure 1.3(a), the lubricating film maintained good condition over a wide area even after the forming process was completed.

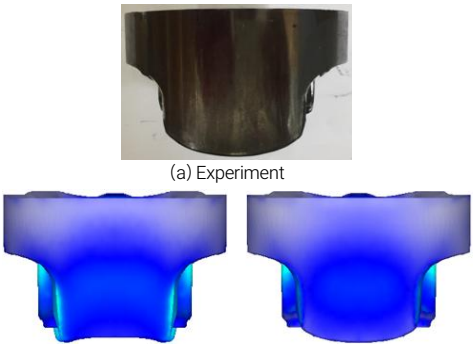

(a) Experiment

(b) Constant friction (c) Functional friction

Fig. 1.3 Three-step forward extrusion process

In conclusion, it can be summarized as follows:

When strain hardening is small, the impact of friction becomes more significant, making friction an important factor in the forming of aluminum, advanced materials, and high-strength materials.The constant shear friction law is suitable for post-lubrication regimes where friction is governed by the deformation of the lubricant film, but since such conditions are rarely met in metal forming, its use should be avoided.While the traditional Coulomb friction law is commonly accepted, in forging, where changes in lubrication regimes are inevitably involved, the use of a variable Coulomb friction law is recommended. In particular, in forward extrusion processes, where the container is long and the cross-sectional reduction is large, lubrication regime changes are significant, so attention should be paid to these changes when analyzing similar processes. The issue in Figure 1.3 broadly falls under this category.

For more detailed information, refer to the following literature.

[1] Wilson, W.R.D., 1978, Friction and lubrication in bulk metal-forming processes. J. Applied Metalworking 1, 7-19.

[2] Lee, S.W.; Lee, J.M.; Joun, M.S.; On critical surface strain during hot forging of lubricated aluminum alloy. Tribol. Int. 2020, 141, 05855.

[3] Hamid, N.A.; Kim, K.M.; Hwang, T.M.; Choi, J.M.; Joun, M.S. Tribological shifting phenomena during automatic multistage cold forging of an automotive Al6082-T6 steering yoke. J. Manuf. Proc. 2024, 114, 178-195.

[4] Heo, Y.; Kim, N.Y.; Nam, J.W.; Chung, I.G.; Joun, M.S. Friction heat ball in round-to-half circle drawing and its effect on the material's skin shearing. Tribol. Int. 2024, 197, 109755.

[5] Joun, M.S.; Moon, H.G.; Choi, I.S.; Lee, M.C.; Jun, B.Y. Effects of friction laws on metal forming processes. Tribol. Int. 2009, 42, 311-319.

[6] Lee, S.W.; Jo, J.W.; Joun, M.S.; Lee, J.M. Effect of friction conditions on material flow in FE analysis of Al piston forging process. Int. J. Precis. Eng. Manuf. 2019, 20, 1643-1652.

2.AFDEX_V24R01 release

The AFDEX_V24R01 version was released in October 2024. This update was introduced in the 2024 Q2 and Q3 newsletters, and the relevant details are summarized here in the 2025 Q1 update.

3. New features in V24R01

3.1 Lubrication damage rate calculation

Friction stress is calculated based on either the Coulomb friction law or the constant shear friction law. The constant shear friction law essentially assumes a constant friction stress, which is not ideal for metal forming applications.

The Coulomb friction law, on the other hand, assumes that the friction stress is proportional to the normal stress on the friction surface. When the state of the friction surface does not change, this can be considered empirically realistic.

However, during plastic deformation, especially in forging processes, the friction surface condition can change rapidly, so using a constant friction coefficient does not reflect the complex phenomena that occur in actual forging. What might seem empirically accurate is often an underestimation of the precision of the forging simulator or a habitual focus on trends.

While the traditional Coulomb friction law, using a constant friction coefficient, may still provide useful predictions from a macroscopic perspective in steel forging, more careful consideration of friction is necessary when quantitatively predicting wear or highly accurate forming loads.

Unlike steel, materials such as aluminum alloys exhibit significantly reduced strain hardening and softening of flow stress due to temperature effects during forging. In these cases, the influence of friction becomes more pronounced. Lee et al. [S. W. Lee, J. M. Lee, M. S. Joun, 2020, On critical surface strain during hot forging of

lubricated aluminum alloy, Trib. Int. 141, 105855] found that, during hot forging of aluminum alloys, the friction coefficient highly depends on the surface strain of the material, and it increases sharply at a certain surface strain. Similarly, Hamid et al. [N. A. Hamid, K. M. Kim, T. M. Hwang, J. M. Choi, M. S. Joun, Tribological shifting phenomena during automatic multistage cold forging of an automotive Al6082-T6 steering yoke, Journal of Manufacturing Processes, V. 114, 2024, 178-195] revealed similar phenomena occurring in the automatic multistage cold forging of a passenger car steering yoke.

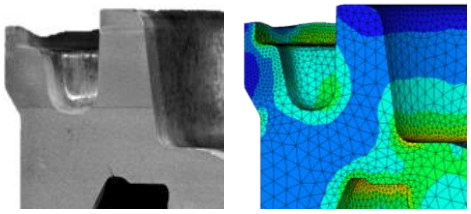

(a) Experiment (b) Prediction

Fig. 3.1 Prediction of wave-like outer shape using lubrication damage rate

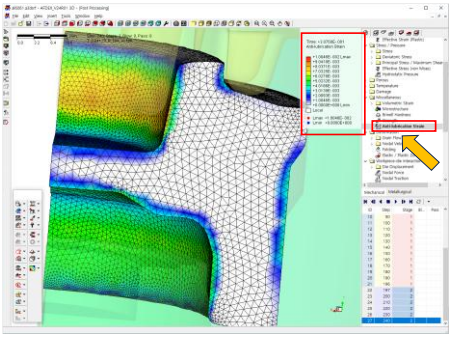

Fig. 3.2 Lubrication damage rate

Figure 3.1 compares the experimental and predicted shapes of wave-like patterns that occur at the side of aluminum alloy during cold forging. It shows a good match between the two. Simply considering the surface strain of the material at the contact surface alone would not be sufficient to achieve such results as shown in the figure.

To obtain prediction results that align with experimental data, the degree of lubricant damage at the friction surface must also be taken into account.

In V24R01, a fundamental feature for this is provided, as shown in Figure 3.2, where the analysis results of the lubrication damage rate can be confirmed.

3.2 Independent die structural analysis

In previous versions, die structural analysis was conducted simultaneously with the forming analysis. Therefore, in older versions, the forming analysis had to be performed first before carrying out the die structural analysis.

In ADFEX V24R01, die structure analysis can be performed independently of forming analysis, using the results of the forming analysis but without being dependent on it. This function allows for die structure analysis of various die designs created based on optimized or validated process designs, enabling die design optimization.Figure 3.3 illustrates the basic concept of this function. The process simulation result in Figure 3.3(a) focuses on the deformation of the material, emphasizing the contact between the material and the die.

Figures 3.3(b) and 3.3(c) show the results of independent die structure analysis, which are conducted separately from the forming analysis using the contact stresses obtained from the forming analysis results in Figure 3.3(a). This function is focused on the optimal design of the die.

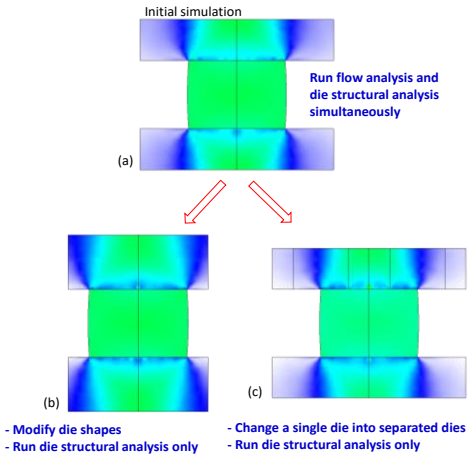

Fig. 3.3 Independent die structure analysis (Die reanalysis function)

3.3 Tensile test, flow curve, and work hardening capability

The material just before forging or metal forming shows significant variations in its properties, such as flow characteristics, depending on the history it has gone through (e.g., drawing, heat treatment). Considering that flow characteristics are a key factor in metal forming processes, the tensile test, which provides detailed information about these characteristics, cannot be overemphasized. It is important to highlight again, given that it is common to encounter incorrect flow characteristics derived from tensile tests in academic papers. The previous version of AFDEX/MAT provided a method to obtain flow curves from tensile tests based on strong plastic finite element methods. Recently, a new flow curve improvement technique using elastoplastic finite element methods has been developed.

Figure 3.4 shows the flow characteristics (Figure 3.4(a)) and work hardening rate (Figure 3.4(b)) of various materials for automatic multi-stage cold forging. Figure 3.4(c) compares the results of tensile test analyses conducted using flow curves obtained from tensile specimens with different gauge length-to-diameter ratios, all analyzed based on the same standard (gauge length-to-diameter ratio = 5).

By comparing the analysis results of standard tensile tests, flow characteristics and forging capability can be verified. What needs to be emphasized once again is that these flow curves vary depending on the material's pre-treatment (e.g., drawing process, heat treatment), so regular tensile testing and flow characteristic assessment are necessary to proactively address potential issues. This process contributes to the accumulation of scientific and technical expertise.

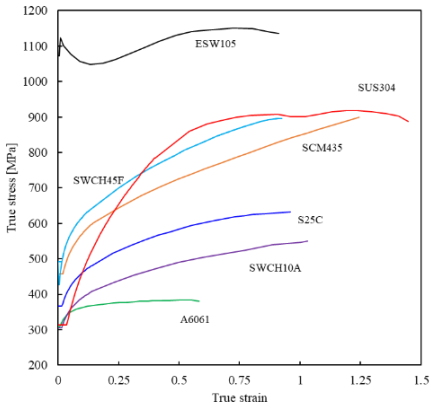

(a) Flow curves obtained from tensile specimens of different specifications

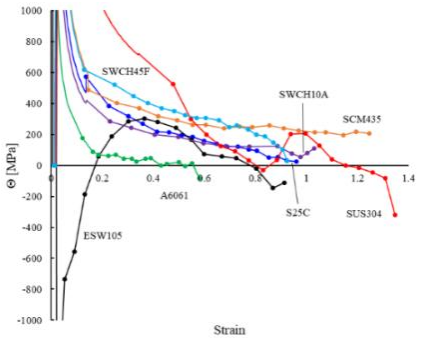

(b) Work hardening capability

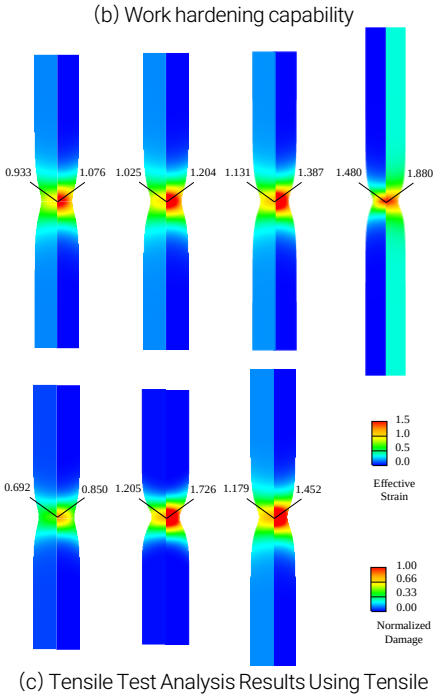

(c) Tensile Test Analysis Results Using Tensile Specimens with the Same Gauge Length-to-Diameter Ratio (5)

Fig. 3.4 Identification of Flow Characteristics from Tensile Test Results

3.4 High accuracy in damage calculation

Mesh reconstruction is essential in the analysis of volumetric metal forming processes, including forging. Mesh reconstruction improves distorted meshes and, if necessary, adjusts them to meet the changed boundary conditions. However, it inherently leads to changes in state variables, including strain and damage. Generally, material deformation tends to occur in a diffusive manner. This phenomenon is influenced by the laws of mass conservation, strain hardening, and strain rate hardening.

However, the degree of damage is different in this case. Ductile fracture occurs partially, and the deformation softening caused by the damage tends to reinforce these characteristics. Therefore, careful attention is required during the process of element density assignment in mesh reconstruction. If such measures are not considered, the obtained damage value may only reflect trends without providing meaningful insights.

According to recent research findings, when the length of the edge segment of an element is about 1/10th of the length of the target crack, a damage value with resistance to mesh reconstruction can be obtained. Figures 3.5(a) and 3.5(b) were presented at the 2014 User Conference (Seongjin Former). The results at that time were qualitatively significant. However, due to the flattening caused by mesh reconstruction, the exact location of crack initiation could not be predicted. Figure 3.5(c) satisfies the aforementioned element density requirements, and as shown in Figures 3.5(d–e), the prediction results align with the experimental results. Figure 3.5(c) holds important significance, as it implies that when the element edge length is below the critical threshold (0.11 mm), the damage value becomes independent of mesh reconstruction.

Tensile testing not only provides the flow curve but also gives information about the critical damage at fracture. Therefore, to examine the element density requirements considering ductile fracture, the correlation between element density and damage value is shown in Figure 3.5(c). This figure indicates that, assuming the element density requirements are met, the critical damage value is 1.15. As seen in Figure 3.5, by utilizing AFDEX's intelligent mesh reconstruction function, it is emphasized that detailed ductile fracture information can be obtained using an appropriate mesh in most cases.

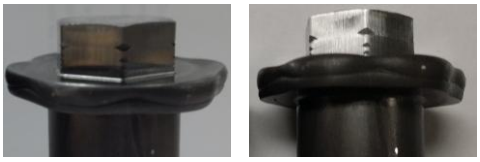

(a) Experiment (Seongjin Former, MFCAE 2014)

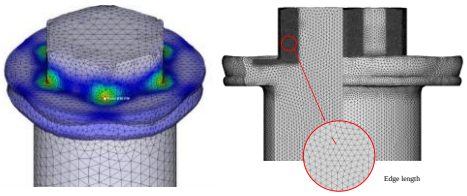

(b) Prediction (Seongjin Former, MFCAE 2014)

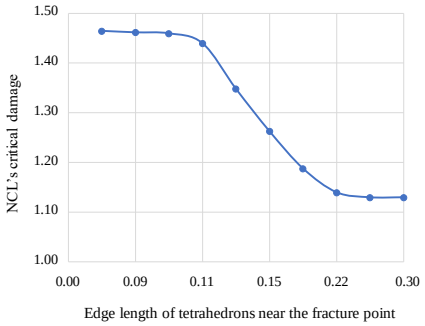

(c) Mesh considering crack length

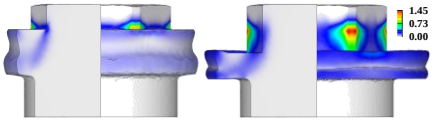

Fracture instant Final stroke

(d) Results meeting the ductile fracture element density requirements

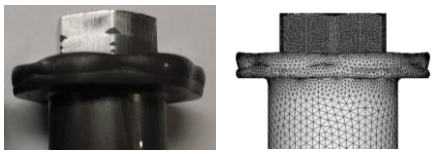

Experiment Prediction

(e) Prediction of wrinkles occurring during bolt head forming

Fig. 3.5 Element edge length vs. maximum fracture damage (tensile test)

3.5 Direct input of die element mesh

The geometric information of a die is typically composed of surface data. This information is discretized into a mesh either by the Pre-Processor or within the program itself for structural and heat transfer analysis of the die. To enhance user convenience, AFDEX incorporates intelligent technology by embedding mesh generation and reconstruction functions into the program. By default, AFDEX uses this function to generate the die's mesh. This function allows sufficient control over the element density when generating the die mesh. This capability is made possible by AFDEX's powerful intelligent mesh reconstruction function. However, there may be instances where the user needs to input the die mesh directly. In such cases, when element mesh data is input instead of the surface data, the program automatically generates the die's surface information and uses the input mesh data for structural and heat transfer analysis. It is important to note that, just like materials, the die's finite element mesh can also flexibly control element density.

Figure 3.6 illustrates a simple application case for conceptual explanation.

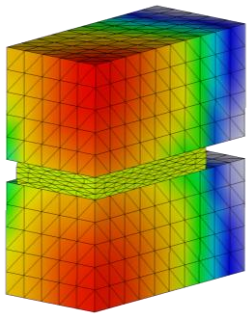

Fig. 3.6 Application case of the input die mesh

3.6 Automatic analysis of drawing process

The drawing process is typically a multi-pass process. However, automatic analysis is not straightforward due to the grip. The traditional method involved applying boundary conditions or positioning an inseparable die beneath the material. This approach made full automation impossible. The new method shapes the grip by applying no deformation or stress to the material using a virtual extrusion process until the grip is created. Afterward, the extrusion conditions are removed, and velocity conditions are applied to the grip to perform the automatic analysis. Complete automation is possible regardless of the number of passes.

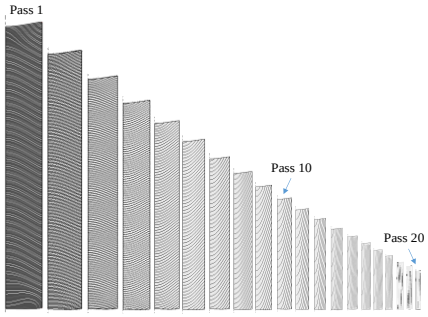

(a) Results after the drawing process

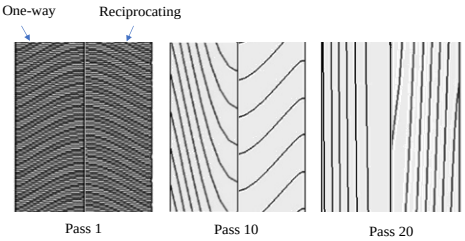

(b) Metal flow curve when the diameter is uniformly enlarged

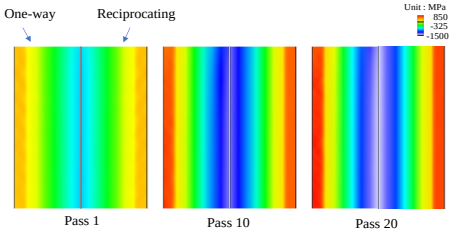

(c) Axial residual stress component

Fig. 3.7 Analysis results of the drawing process

Mesh reconstruction is crucial in the analysis of the drawing process. It is essential due to the increase in calculation time caused by the elongation of the material, unexpected deformation occurring in the grip area, and poor material

material-die contact as the number of passes increases. In mesh reconstruction for the drawing process, factors such as the simplicity of the material shape and element density must be considered. A key issue in the analysis of the drawing process is that residual stresses are concentrated on the surface. Compared to the strain distribution on the surface, the distribution of residual stresses changes dramatically. To take advantage of this characteristic, using structural elements in 2D and applying directional skin dense meshes in 3D is effective. Figure 3.7 shows an application case for a 20-pass bar drawing process. The cross-sectional reduction rate for each pass is uniformly 10%. Figure 3.7(a) presents the final shape of each pass at a 1:1 scale, while Figure 3.7(b) enlarges the exit lines of the 1st, 10th, and 20th passes to the same size. On the left side of Figure 3.7(b) is the predicted result for a unidirectional drawing process, and on the right side is the result for a bidirectional drawing process. The left side of Figure 3.7(c) shows the axial residual stress component at the end of both the unidirectional and bidirectional drawing processes. The similarity between the two results indicates that the residual stress from the previous stage does not significantly affect the drawing process at the current stage.

3.7 Simultaneous compensation of high-temperature flow curves, temperature, and friction

High-temperature cylinder compression tests are widely conducted to obtain the flow characteristics of materials. When aiming to obtain accurate high-temperature flow curves, both temperature and friction issues arise. In reality, high-temperature compression tests are conducted under non-isothermal conditions. While they are often referred to as isothermal, the plastic deformation heat generated during the compression test prevents actual isothermal conditions from being maintained. The temperature rise during the compression test varies depending on the material, with titanium alloys being an extreme case. This is due to their high strength, relatively low heat capacity, and delayed thermal conductivity. The true stress-strain curve, or ideal flow curve, can be calculated assuming displacement-compression load occurs under isothermal and frictionless conditions. The ideal flow curves of materials such as magnesium and titanium alloys show significant differences from the actual flow curves. Therefore, compensation for friction and temperature is necessary. In other words, errors arising from the assumption of frictionless and isothermal conditions must be corrected.

Figure 3.8 shows the flow curve for the magnesium alloy AZ80A, where the solid line represents the ideal flow curve, and the dashed line represents the model derived from the equation. The final flow curve, obtained by applying temperature compensation to this model, is shown as a dotted line. When the compression test was analyzed using this flow curve, sufficiently accurate compression load-stroke results were obtained. Magnesium alloys exhibit a large difference in flow stress with temperature, so even small temperature changes significantly affect the flow stress. The influence of friction is relatively small, so compensation for friction is not necessary. Although friction increases flow stress at the contact surface, the contact area remains large under frictionless conditions, thus offsetting the impact on the compression load. However, the case is different for aluminum. The effects of temperature and friction are similar in magnitude. Generally, when temperature effects are considered, flow stress increases, while friction effects tend to decrease flow stress.

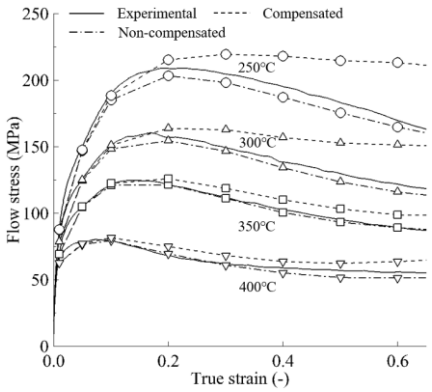

Fig. 3.8 Flow curve of AZ80A at a strain rate of 1 (1/s)

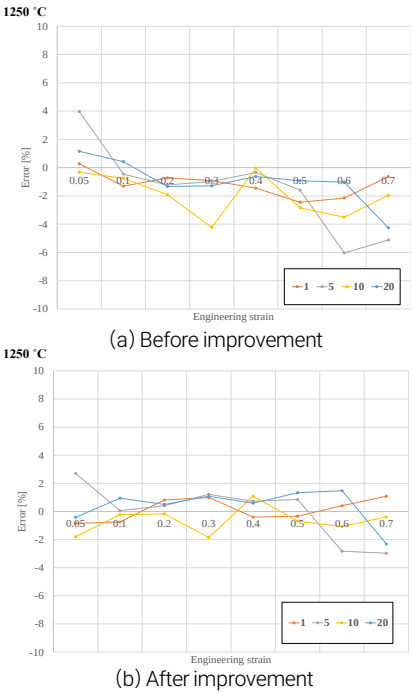

(a) Before improvement

(b) After improvement

Fig. 3.9 Simultaneous Compensation for Temperature and Friction

As mentioned earlier, aluminum alloys exhibit relatively small temperature compensation effects (due to their fast thermal conductivity), making friction compensation more important. Since the effects of these two factors on flow stress are not absolute, both friction and temperature effects must be compensated for. Compensation for friction is somewhat more complex compared to temperature compensation. In reality, both influences affect the process collectively, and thus, simultaneous compensation for both temperature and friction is necessary. The simultaneous temperature and friction compensation technique using AFDEX has been established. Figure 3.9 shows the error in the flow curve obtained using AFDEX's high-temperature flow curves. As seen in Figure 3.9(a), the error is minimized and controlled to a low level during the flow curve acquisition stage. When the latest simultaneous temperature and friction compensation method is applied, as shown in Figure 3.9(b), both the average error (reduced from 2.4% to 1.8%) and the maximum error (reduced from 6% to 3%) are significantly reduced.

3.8 Change of pre-processor and post-processor icons

In V24R01, the pre-processor and post-processor icons have been modified to better reflect the characteristics of the analysis condition input. The modified pre-processor icons can be seen in Figure 3.10.

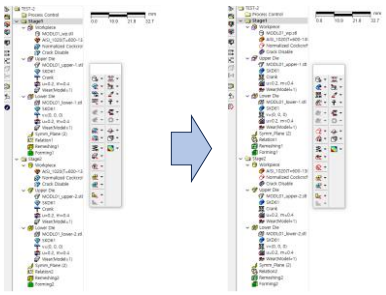

Fig. 3.10 Change of pre-processor icons

3.9 Stress triaxiality display feature

V24R01 will provide a feature for displaying stress triaxiality, which is the ratio of hydrostatic stress to equivalent stress. This feature can be accessed from the stress tab under the post-processor's sub-menu, as shown in Figure 3.11.

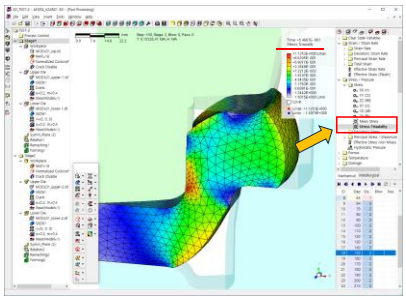

Fig. 3.11 Stress triaxiality display feature

3.10 User defined description input function

V24R01 introduces a new feature that allows users to enter detailed descriptions of their analysis tasks. To resolve the inconvenience of writing descriptions in file or folder names, a description field has been added to the AFDEX project file. Multilingual input, including English, Korean, and Japanese, is supported.

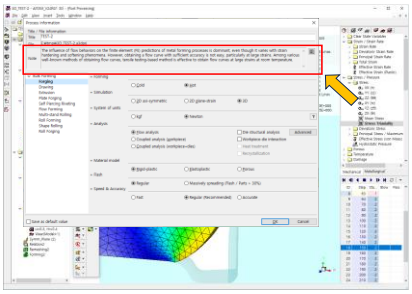

Fig. 3.12 User Description Input

3.11 Pre-processor function for roll forging process analysis

Up until the AFDEX_V23R02 version, when performing roll forging (Roll forging) process analysis, users would first create the basic conditions for the process analysis using the pre-processor, and then input the boundary conditions for the rolls and materials in a text editor. In the AFDEX_V24R01 version, as shown in Figure 3.13, all input data can now be created directly in the pre-processor, improving user convenience.

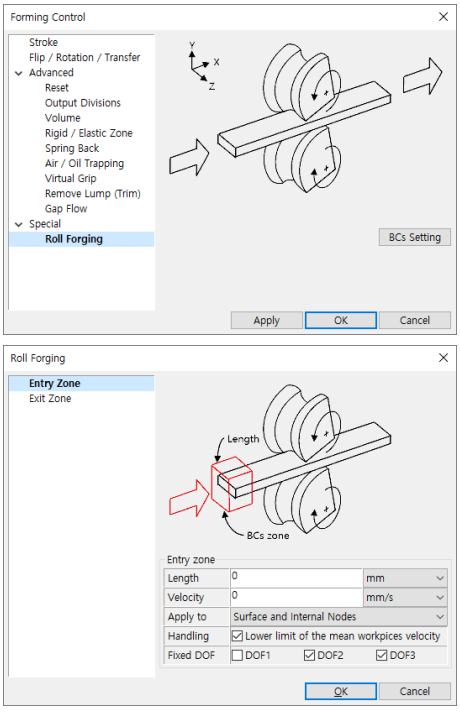

Fig. 3.13 Roll forging process analysis condition input UI

3.12 Contact area display function in multi-object analysis

In the AFDEX_V23R02 version, it was not easy to verify the contact areas between objects from the results of multi-body analysis. In the AFDEX_V24R01 version, the contact areas between all objects, including die-material as well as material-material, are displayed. Figure 3.14 shows an example applying this new function to a case where three objects are deformed by two dies and one binder. The contact between different objects can be visually confirmed by different colors. The two colors at the bottom indicate the contact status between the three deformed bodies.

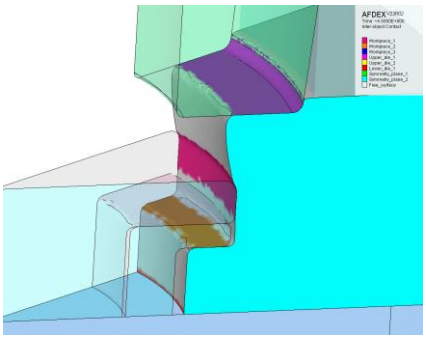

Fig. 3.14 Contact area display screen between objects

4. Improvements in V24R01

4.1 Prediction of die overheating during shape drawing

In most metal forming processes, including forging, frictional heat is not considered critical. Of course, friction itself is important. Therefore, in most forging simulations, attention is not paid to frictional heat. The situation is quite different in the drawing process. In drawing, the material continuously contacts a specific area of the drawing die, causing relative motion and slippage. For this reason, lubrication is required continuously, and lubricants and additives for drawing are used. However, depending on the situation, there are limits to how well lubricants can solve the problem of die overheating that may occur in shape drawing.

Starting from the AFDEX_V24R01 version, users can directly control frictional heat, and by utilizing the temperature-dependent friction coefficient input feature already provided, the prediction of die overheating, i.e., the friction heat ball, in circular-semicircular shape drawing processes has been made possible.

Figure 4.1 shows the overheating of the die caused by frictional heat after 5 seconds from the start of drawing, with a maximum temperature of 160° C. This overheating is caused by frictional heat generated in a narrow region. Considering the actual process time and the vicious cycle of frictional heat, temperature rise, and friction, the maximum temperature can significantly increase.

The overheated friction heat ball rapidly increases the surface temperature of the incoming material and causes a sharp thermal softening of the flow stress at the surface. This can lead to surface flow, and as shown in Figure 4.2, unexpected overlap defects may form at the corner of the deformed material, which are not intuitively understandable. Such extreme phenomena are more likely to occur in high-strength and high-thermal-softening materials.

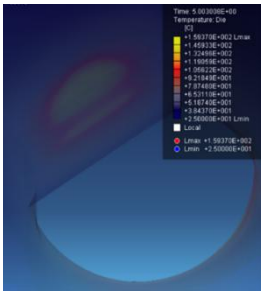

Fig. 4.1 Overheating of the drawing die due to frictional heat

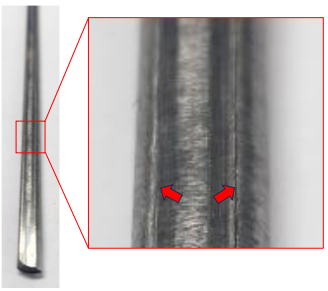

Fig. 4.2 Overlap defects occurring in the circular-semicircular shape drawing process

4.2 Improvement in calculation time (Example: rotating die)

In previous versions, when using a rotating die, there was an issue with excessive contact area checking time. As a result, the calculation efficiency of processes such as roll forging and pilgering was lower compared to other processes.In V24R01, by optimizing the contact area checking function for rotating dies, the time required for simulations has been significantly reduced. Figure 4.3 compares the simulation time for the roll forging process between the previous and the latest versions.

Fig. 4.3 Comparison of calculation time differences

4.3 AFDEX /MAT Function improvements

In response to the increasing use of AFDEX/MAT, several improvements have been made. Some of them are summarized as follows:

- Raw data input functionality
- Curve fitting functionality
- Solution step input functionality for tensile analysis using the cold 8th equation model
- Functionality to save yield stress and stroke for room temperature tensile test input files

-Raw data extraction from high-temperature compression test graphs for List control window output

4.4 STL Export function improvements and changes

In previous versions, when performing the STL export, multiple objects were saved in a single file. This could lead to errors when using the STL file in 3D CAD software that did not support this functionality. In V24R01, as shown in Figure 4.4, the function has been improved to allow for exporting each object with a different file name.

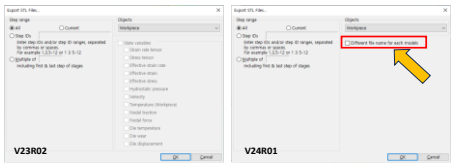

Fig. 4.4 Improved stl export dialog

4.5 Binder load information input function improvements

Previously, binder load was entered as a function of absolute time or distance. In V24R01, binder load can now be entered as a function of relative displacement between the binder and die. As shown in Figure 4.5, the pre-processor input window has been updated to allow input of load information based on compression distance or relative displacement for various binder/spring die conditions

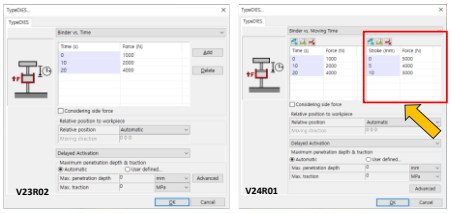

Fig. 4.5 Example of binder load input information

4.6 Automatic range determination method for analysis results in postprocessor

In previous versions, when performing simultaneous analysis for multiple objects, the legend range for analysis results (e.g., stress, strain) was determined based on the minimum and maximum values across all objects, regardless of the selected visualization object. In V24R01, the legend range is determined based on the minimum and maximum values of the analysis results for the selected object(s) for visualization.

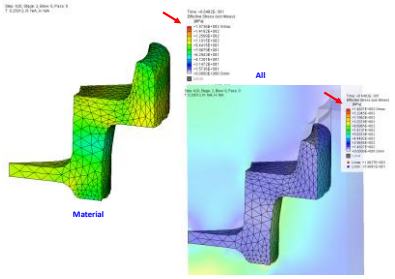

Fig. 4.6 Analysis results for selected objects

4.7 Improved 3D STL model error checking functionality

The AFDEX analysis models for materials and dies use STL files. For proper simulation, the model must not contain surface open or non-manifold errors. Up to AFDEX V23R02, non-manifold errors caused by points were not detected, which led to unidentified errors during simulation. In V24R01, this feature is now supported, and non-manifold errors are detected. Figure 4.7 shows an example where a non-manifold error is detected in the 3D STL model.

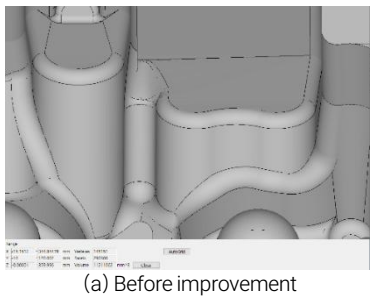

(a) Before improvement

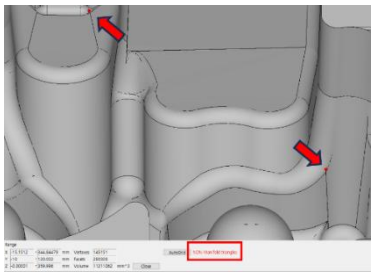

(b) After improvement

Fig. 4.7 3D model error check screen

4.8 Automatic die position initialization feature

In previous versions, the accuracy of edge contact calculations between objects varied depending on the mesh resolution of the shape information. In V24R01, the method for calculating edge contact between objects has been improved, reducing errors in the automatic die position initialization feature. Figure 4.8 demonstrates the improvements in the automatic die position initialization.

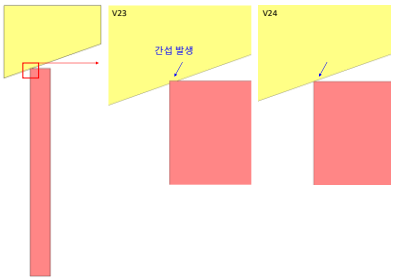

Fig. 4.8 Example of automatic die position initialization

4.9 Velocity field component display in postprocessor

Previous versions provided functionality to view the velocity field components XX, YY, ZZ, and XYZ. Based on user requests, V24R01 introduces a new feature to view two components simultaneously: XY, YZ, and ZX. This feature can be accessed under the velocity tab in the postprocessor's submenu, as shown in Figure 4.9.

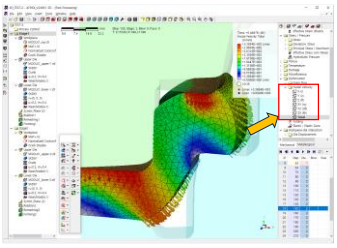

Fig. 4.9 Velocity field component display

4.10 New display types for overall process analysis results

In previous versions, individual shading, mesh, and outline displays were available for selected materials or dies in the analysis results. From V24R01, users can now view shading, mesh, and outline display types for materials or dies in the entire multi-step process. This feature is accessible via the display tab icon shown in Figure 4.10.

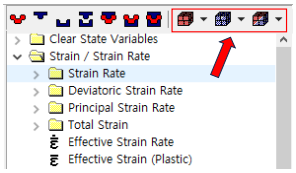

Fig. 4.10 Display type addition icon

4.11 New coulomb friction condition input UI

V24R01 provides a new user interface for inputting dual Coulomb friction conditions. The new friction condition input da[illegible] in Figure 4.11.

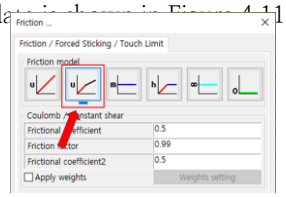

Fig. 4.11 Dual Coulomb friction condition

4.12 Network license activation

In previous versions, AFDEX licenses were provided in a node-locked format. Based on user demand for network licenses, V24R01 introduces a floating license type for network licenses. Even users with the existing dongle key will now use the floating license system.

4.13 Multi-monitor usability improvements

When using multiple monitors, AFDEX's preprocessor pop-up dialogs occasionally did not function correctly depending on the location of the main and parent monitors. This issue has been resolved, and improvements have been made to the starting position and screen size errors in Windows. Additionally, the current monitor position and size are now remembered, improving the user experience.